Accounting for Epistemic Uncertainty in Site Effects in Probabilistic Seismic Hazard Analysis

Kristin J. Ulmer*[1], Adrian Rodriguez-Marek[2], and Russell A. Green[2]

ABSTRACT

A probabilistic seismic hazard analysis performed for rock conditions and modified for soil conditions using deterministic site amplification factors does not account for uncertainty in site effects, which can be significant. One approach to account for such uncertainty is to compute a weighted average amplification curve using a logic tree that accounts for several possible scenarios with assigned weights corresponding to their relative likelihood or confidence. However, this approach can lead to statistical smoothing of the amplification curve and possibly to decreased computed hazard as epistemic uncertainty increases. This is against the expected trend that higher uncertainty leads to higher computed hazard, thus reducing the incentive for practitioners to characterize soil properties at a site. This study proposes a modified approach in which the epistemic uncertainty is captured in a plot of amplification factors versus period. Using a case history, the proposed method is shown to improve the issue with the weighted average method for at least two oscillator periods and to yield similar results for two other periods in which the highlighted issue is less significant.

KEY POINTS

- Handled in a certain way, epistemic uncertainty in site response in a PSHA can lead to unexpected trends.
- The proposed method aligns with the guiding principle that higher uncertainty should lead to higher hazard.
- These results suggest a way to incorporate the uncertainty in the predominant period in the logic tree.

INTRODUCTION

Often, probabilistic seismic hazard analysis (PSHA) is performed for rock conditions and then modified for site effects using deterministic site amplification factors. However, this does not account for uncertainty in site effects, which can be significant. Several approaches have been proposed to incorporate this uncertainty into PSHA (Cramer, 2003; Bazzurro and Cornell, 2004b; Goulet and Stewart, 2009). Moreover, the Electrical Power Research Institute (EPRI) has proposed methods for quantifying epistemic uncertainty in a guidance document, herein referred to as the SPID (i.e., Screening, Prioritization, and Implementation Details; EPRI, 2012).

Uncertainties can generally be divided into two types: aleatory variability and epistemic uncertainty. Aleatory variability is the apparent randomness associated with natural processes and can only be quantitatively refined using additional data and improved understanding of the underlying physical processes, but it cannot be reduced to zero. Epistemic uncertainty is uncertainty associated with a lack of information or knowledge about a process, and theoretically it can be reduced with enough data and understanding of the underlying physical processes. Although conceptually epistemic uncertainty and aleatory variability are distinct, separating the two is often difficult (Der Kiureghian and Ditlevsen, 2009), particularly for site effects. However, the previous definitions can be tied to the parameterization of a given problem, which then makes this separation much clearer. For example, if site effects are parameterized through a parameter vector $\boldsymbol{\theta}$ (say, e.g., average shear-wave velocity over the top 30 m, V_{S30}, and depth to bedrock), any site effects that are a function of other variables weakly correlated to $\boldsymbol{\theta}$ would result in aleatory variability. This is because no effort on the part of the analyst could reduce this uncertainty without changing the model (i.e., increasing the parametric space of $\boldsymbol{\theta}$). On the other hand, uncertainties in the value of $\boldsymbol{\theta}$, or any bias in the site effect models, would fall into the epistemic uncertainty category because additional knowledge would be able to reduce this error.

A general guiding principle in quantifying epistemic uncertainty is that limited information should lead to larger estimated uncertainty. An associated implication is that higher

1. Southwest Research Institute, San Antonio, Texas, U.S.A., https://orcid.org/0000-0001-8696-7447 (KJU); 2. The Charles Edward Via, Jr. Department of Civil and Environmental Engineering, Virginia Tech, Blacksburg, Virginia, U.S.A., https://orcid.org/0000-0002-8384-4721 (AR-M)

*Corresponding author: Kristin.ulmer@swri.org

Cite this article as Ulmer, K. J., A. Rodriguez-Marek, and R. A. Green (2021). Accounting for Epistemic Uncertainty in Site Effects in Probabilistic Seismic Hazard Analysis, *Bull. Seismol. Soc. Am.* **XX**, 1–16, doi: 10.1785/0120200343

epistemic uncertainty should result in a wider spread of hazard fractiles and, consequently, higher mean seismic hazard for typical exceedance rates of interest. However, as will be shown herein, there are scenarios in which having lower uncertainty (i.e., well-characterized site conditions) leads to higher mean ground motions when uncertainty in site response is captured by simple scaling of the small-strain shear-wave velocity (V_S) profile at a site. Although this result can be explained through probability theory (as explained later), it runs counter to the guiding principle postulated earlier and removes some of the incentive for practitioners to perform thorough site characterizations.

The objective of this study is to develop an approach to align the current methods of incorporating epistemic uncertainty into site effects in a PSHA with the guiding principle that higher epistemic uncertainty should lead to seismic hazard estimates that are equal to, or greater than, the hazard estimates associated with lower epistemic uncertainty. First, the common scaling approach will be summarized and potential issues highlighted. A modification to this method will then be proposed, and analysis of a case history will show that using the common scaling approach can lead to higher mean ground motions for lower epistemic uncertainty and that using the proposed modification reverses this trend or lessens this issue. This study focuses on the effects of epistemic uncertainty (usually handled via logic trees) and does not address the effects of aleatory variability.

EXISTING METHODOLOGIES FOR INCORPORATING EPISTEMIC UNCERTAINTY IN SITE RESPONSE

Epistemic uncertainties in site response can be split into those related to model error and those related to the material properties of the site profile. In this article, we focus entirely on the latter; a comprehensive discussion of model error can be found in Stewart and Afshari (2020). Three main sources of epistemic uncertainty for a soil site are the site kappa, stiffness of the soil profile (i.e., the V_S profile), and the nonlinear dynamic properties of each soil strata (e.g., the appropriate modulus reduction and damping [MRD] curves). For the purposes of this study, only the latter two are considered explicitly; uncertainty in the site kappa is included via the uncertainty in small-strain stiffness implicit in the MRD curves. The MRD curves specify the values of the shear modulus ratio ($G/G_{\max}$, in which G is the shear modulus and $G_{\max}$ is the G for small strains, $<10^{-4}$%) and damping as a function of shear strain (γ). In an equivalent-linear site-response analysis, the V_S profile and MRD curves are critical components in estimating the amplification or deamplification of ground motions due to the layers of soil between the assumed elastic half-space (i.e., bedrock) and the ground surface. There are several published MRD curves to choose from, and there are many methods to estimate or measure V_S, each with its own level of uncertainty in the results. Moreover, even if MRD curves are measured for a particular site, there are potential measuring uncertainties that need to be accounted for (Darendeli, 2001). To account for the uncertainties in V_S and MRD curves, a logic tree can be used to consider several scenarios with assigned weights representing the estimated likelihood of, or confidence in, each scenario based on judgment or experience (Rodriguez-Marek *et al.*, 2020).

Uncertainty in the V_S profile

Although there is more than one way to incorporate epistemic uncertainty in site-response analyses, this study will rely on the guidance in the SPID because it is the method commonly adopted for critical facilities, and hence, it is seen as a reference point for hazard analysis. To account for uncertainty in the V_S profile, the SPID recommends a scaling approach that establishes three V_S profiles: a best estimate (or median) profile derived from measurements or correlations, a lower-range estimate, and an upper-range estimate. A common choice is that the lower- and upper-range estimates represent the 10th and 90th percentiles, respectively, which are created by decreasing or increasing the median V_S profile by 1.282 times the standard deviation ($\sigma_{\ln V_S}$), assuming a lognormal distribution of V_S, with weights of 0.4 for the central branch and 0.3 for the other two branches. This choice represents a three-point representation of a continuous lognormal distribution (Keefer and Bodily, 1983). The SPID recommends $\sigma_{\ln V_S} = 0.35$ when very limited geotechnical or geophysical site investigation data are available and $\sigma_{\ln V_S} = 0.50$ when non-site-specific information is used (e.g., correlations with geological information, and so forth). Lower values of $\sigma_{\ln V_S}$ are allowed for well-characterized sites with multiple measurements. Figure 1 illustrates what the median, lower-range, and upper-range profiles might be for a hypothetical scenario. This hypothetical scenario will be used to illustrate the SPID method and to highlight the issues with its implementation.

There are other aspects of the V_S profile that can introduce uncertainty in the site response, including the depth to bedrock, depth to intermediate impedance contrasts, and presence of soft soil layers. In principle, this uncertainty is also uncertainty in the V_S profile, but these cannot be handled through scaling the median V_S profile as outlined in the SPID. We strongly recommend that these sources of uncertainties be represented to fully capture the epistemic uncertainty. A possible way of doing so is by building a multinode logic tree that includes nodes that represent each source of uncertainty (e.g., Rodriguez-Marek *et al.*, 2020).

Uncertainty in nonlinear dynamic soil properties

To account for uncertainty in the nonlinear dynamic soil properties, the SPID recommends that two sets of MRD curves be used. These curves should be selected to reasonably reflect the range in nonlinear dynamic soil properties at the site. The SPID recommends using the EPRI (1993) and Peninsular Range (Silva *et al.*, 1996; Walling *et al.*, 2008) curves, though

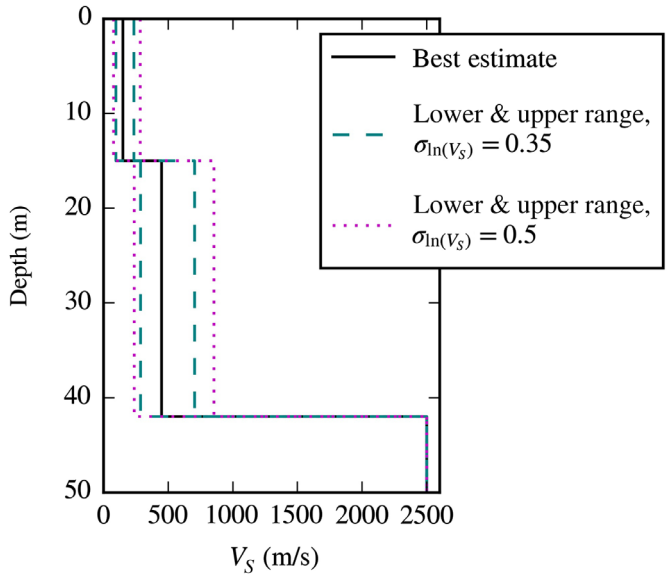

Figure 1. Best estimate, lower- and upper-range V_S profiles (i.e., median, 10th and 90th percentiles) for a hypothetical scenario where $\sigma_{\ln V_S} = 0.35$ or $\sigma_{\ln V_S} = 0.5$. This hypothetical scenario is used in subsequent figures. The color version of this figure is available only in the electronic edition.

other published curves are acceptable (e.g., Ishibashi and Zhang, 1993; Darendeli, 2001) and, in the opinion of the authors of this study, better represent the stress-dependent behavior of the soil than the EPRI recommended curves. Regardless, the authors appreciate that the Darendeli and Stokoe (Darendeli, 2001) and Ishibashi and Zhang (1993) MRD curves, which are used in the analyses herein, at present may not capture the range of technically defensible MRD curves. Figure 2 shows examples of two sets of MRD curves that can be used directly in equivalent-linear site-response analyses or to calibrate more advanced nonlinear models, if desired. This study will focus primarily on equivalent-linear methods. In the logic tree, the SPID recommends that each MRD curve be given an equal weight (0.5), though this could be adjusted based on judgment.

Weighted average amplification curves using the logic tree

An example logic tree to account for epistemic uncertainty in site effects is shown in Figure 3. As shown in this figure, nodes are used when competing models are available (e.g., competing MRD models or V_S profile models), and the sum of the weights for the branches emanating from a given node is equal to 1.0, which must be maintained if the weights are adjusted. In this study, the logic tree contains six terminal branches (or leaves), but this could be increased for cases in which the site characterization includes additional complexities. For example, additional scenarios might consider different depths to bedrock, different depths to some of the impedance contrasts, or the presence or absence of a given layer (e.g., a soft soil layer).

As recommended in the SPID, the logic tree with its branches and associated weights is then used to develop a weighted average amplification curve. The amplification curve relates the 5% damped spectral acceleration at the surface of the soil profile (SA_{Soil}) to the 5% damped spectral acceleration at bedrock (SA_{Rock}) through a period-dependent amplification factor: $AF(T) = SA_{\text{Soil}}(T)/SA_{\text{Rock}}(T)$, in which T is the period of a single-degree-of-freedom linear-elastic oscillator. For simplified notation in future equations, these variables will be written as $X = SA_{\text{Rock}}(T)$, $Y = AF(T)$, and $Z = SA_{\text{Soil}}(T)$ (i.e., $Y = Z/X$). The value of AF may be computed using equivalent-linear analysis with a suite of input ground motions at bedrock. The SPID recommends that 11 expected (median) peak acceleration values at reference rock are needed to span from 0.01g to 1.50g. If the analyst chooses to use the random vibration theory, then 11 input Fourier spectra and associated response spectra are sufficient for the site-response analyses. However, if time histories are used, it is likely that multiple time histories for each median peak acceleration value

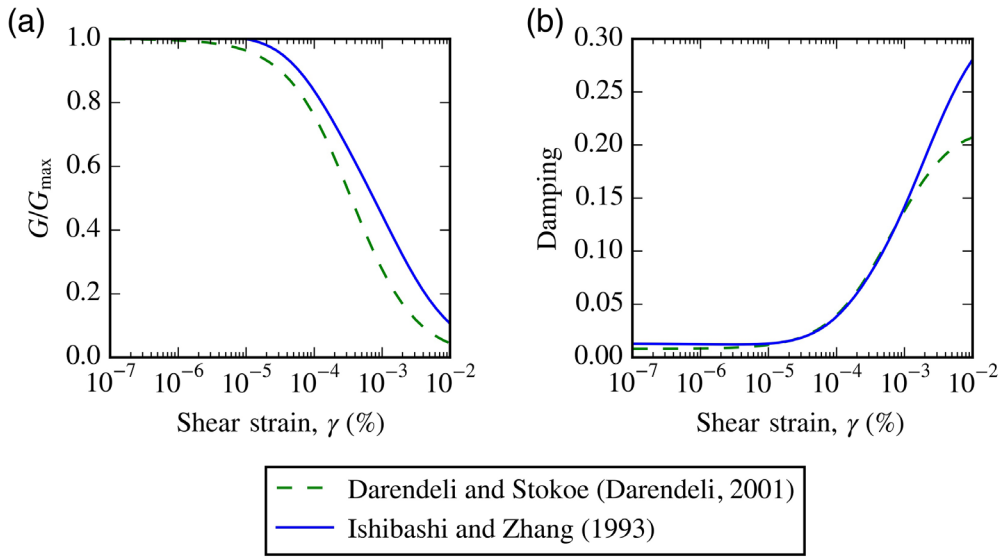

Figure 2. Example modulus reduction and damping (MRD) curves, (a) $G/G_{\max}$ and (b) damping, for the hypothetical scenario (in which the plasticity index is 0 and mean effective stress is 100 kPa). The color version of this figure is available only in the electronic edition.

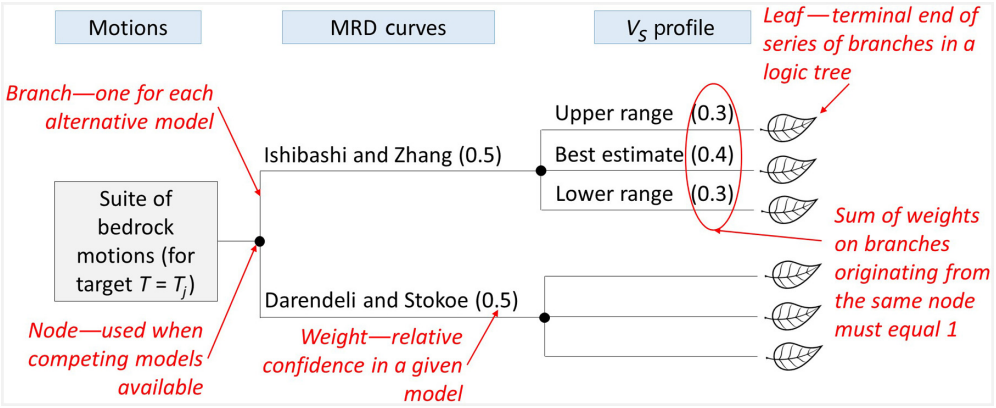

Figure 3. Example logic tree based on Screening, Prioritization, and Implementation Details (SPID) recommendations for the hypothetical scenario. Note that T_j is the target oscillator period. The color version of this figure is available only in the electronic edition.

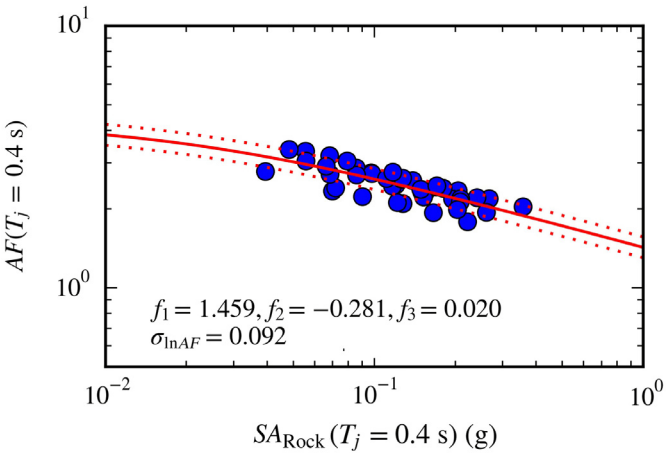

Figure 4. Example of a nonlinear relationship between $AF(T)$ and $SA_{\mathrm{Rock}}(T)$ representing a series of branches terminating in a leaf on the logic tree for the hypothetical scenario. The color version of this figure is available only in the electronic edition.

will be required. However, for the illustrative analyses presented subsequently, only 11 ground-motion time histories were used (e.g., Stewart *et al.*, 2014).

For each scenario in the logic tree (i.e., each series of branches ending in a leaf), site-response analyses of the suite of input ground motions will result in a range of $AF(T)$ values. In some cases, the relationship between $\ln[AF(T)]$ and input ground-motion intensity (e.g., SA_{Rock}) will be nonlinear, which will result in an intensity-dependent mean ($\mu_{\ln Y|X}$). The mean is fitted to the $\ln[AF(T)]$ versus $SA_{\mathrm{Rock}}(T)$ data as shown in Figure 4 and as defined in the following equation (Stewart *et al.*, 2014):

$$\mu_{\ln Y|X} = f_1 + f_2 \log\left(\frac{X + f_3}{f_3}\right), \tag{1}$$

in which f_1, f_2, and f_3 are model parameters regressed to fit the $AF(T)$ versus $SA_{\mathrm{Rock}}(T)$ data. The parameter f_3 constrains the value of SA_{Rock} in which nonlinearity starts to impact the AF; this parameter often cannot be determined from the regressed data, so an assumed value is used (Stewart *et al.*, 2014). In other cases, the relationship will be linear, which will result in an intensity-independent mean ($\mu_{\ln Y|X} = \mu_{\ln Y}$), which is equivalent to $f_2 = 0$.

A weighted average of the $\mu_{\ln Y|X}$ functions obtained from each branch in the logic tree is computed as

$$\mu_{\mathrm{Total}} = \sum_i w_i \mu_i, \tag{2}$$

in which w_i is the weight associated with scenario i, μ_i is $\mu_{\ln Y|X}$ for scenario i, and μ_{Total} is the weighted average of $\mu_{\ln Y|X}$ representing the entire logic tree. The weighted average of the standard deviation of $AF(T)$ is computed as

$$\sigma_{\mathrm{Total}} = \sqrt{\sum_i w_i[(\mu_i - \mu_{\mathrm{Total}})^2 + \sigma_i^2]}, \tag{3}$$

in which σ_i is the standard deviation of $AF(T)$ ($\sigma_{\ln Y|X}$) for scenario i and σ_{Total} is the weighted average of $\sigma_{\ln Y|X}$ representing the entire logic tree. Equations (2) and (3) might have to be applied to different intensity levels to capture the nonlinearity shown in Figure 4. For the purposes of this study, σ_i is assumed to be zero because it is assumed to be a component of aleatory variability rather than epistemic uncertainty.

A plot of AF versus T is shown in Figure 5 for the hypothetical example corresponding to the profiles shown in Figure 1 and the logic tree shown in Figure 3. This plot does not sample AF as a function of SA_{Rock}. In addition, a plot of σ_{Total} versus T is shown in this figure. Observe how the σ_{Total} curve is not smooth and shows localized regions of very low uncertainty. This is because for some periods the AF values have a narrow range of uncertainty due to the individual scenarios, in a plot of AF versus period, crossing each other. This result is only an artifact of the three-point representation of the epistemic uncertainty in V_S profiles. To avoid underrepresenting epistemic uncertainty, we strongly recommend that the relationship between σ_{Total} and T be smoothed across T (Fig. 5). Implicit in this recommendation is that the epistemic uncertainty for site response ultimately must be evaluated in

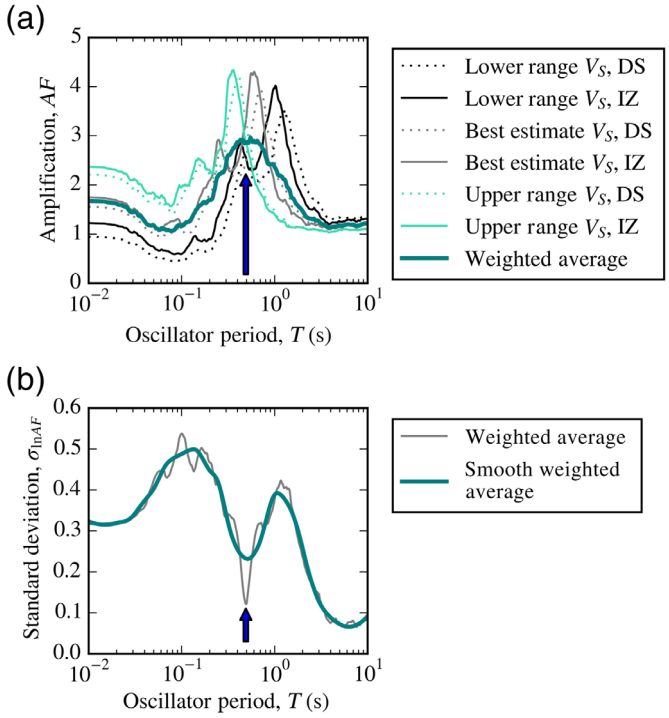

Figure 5. Example plots of (a) $\exp(\mu_i)$ and $\exp(\mu_{\text{Total}})$ versus T and (b) σ_{Total} and smoothed σ_{Total} versus T for the hypothetical scenario. IZ: Ishibashi and Zhang (1993) MRD curve and DS: Darendeli and Stokoe (Darendeli, 2001) MRD curve. Arrows indicate the period at which σ_{Total} reaches a deceptively low value. The color version of this figure is available only in the electronic edition.

terms of the resulting amplification factors and not simply through a logic-tree representation of the underlying site profile.

Probabilistic site-specific soil hazard curves for SA_{Soil}

The weighted average $AF(T)$, as characterized by μ_{Total} and σ_{Total}, is used to develop probabilistic site-specific soil hazard curves for SA_{Soil} at a target oscillator period, T_j. Using the convolution approach of Bazzurro and Cornell (2004b); also proposed as approach 3 in the SPID), the annual rate of exceedance, λ_z, of an arbitrary level of $SA_{\text{Soil}}(T_j)$ is computed as

$$\lambda_z(a) = \int_0^\infty P\left[Y \geq \frac{a}{x}|x\right] f_x(x)dx, \tag{4}$$

in which a is an arbitrary level of $SA_{\text{Soil}}(T_j)$, $P[Y \geq \frac{a}{x}|x]$ is the probability that $AF(T_j)$ is greater than a/x given $x = SA_{\text{Rock}}(T_j)$, and $f_x(x)$ is the probability density function of $SA_{\text{Rock}}(T_j)$.

Equation (4) can be written in discretized form as

$$\sum_{x_k} P[Y \geq \frac{a}{x_k}|x_k]p_x(x_k), \tag{5}$$

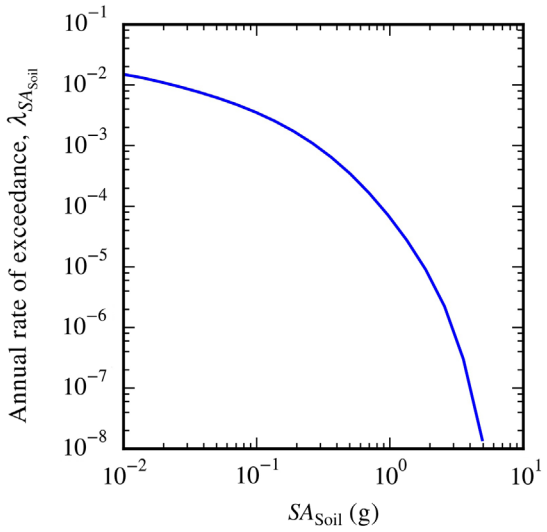

Figure 6. Example probabilistic site-specific soil hazard curve for the hypothetical scenario ($T_j = 0.4$ s). The color version of this figure is available only in the electronic edition.

in which $p_x(x_k)$ is the annual probability of occurrence for $SA_{\text{Rock}}(T_j)$ at discrete values of x_k from a PSHA for rock (e.g., U.S. Geological Survey [USGS], "Unified Hazard Tool," see Data and Resources). Then, $P[Y \geq \frac{a}{x_k}|x_k]$ can be computed assuming $AF(T_j)$ is lognormally distributed with a mean of μ_{Total} and standard deviation of σ_{Total}:

$$P\left[Y \geq \frac{a}{x_k}|x_k\right] = 1 - \Phi\left(\frac{\ln(\frac{a}{x_k}) - \mu_{\text{Total}}}{\sigma_{\text{Total}}}\right), \tag{6}$$

in which Φ is the standard Gaussian cumulative distribution function. Repeating the calculation for several values of a develops a soil hazard curve: λ_z versus SA_{Soil}. Caution should be exerted when convolving total mean amplification with the total standard deviation. In some cases, this may produce inflated surface hazard at some frequencies, compared with the approach of convolving the rock hazard with the amplification functions at the end of each logic-tree branch and using the weights from the logic tree to combine the surface hazard curves at a given frequency.

An example of the resulting probabilistic site-specific soil hazard curve is shown in Figure 6. This hypothetical scenario uses for its rock hazard curve an assumed circular area source (1000 km radius, **M** 5.0–8.5), a Gutenberg–Richter b-value equal to 1, and a recent ground-motion model (i.e., Chiou and Youngs, 2014) to estimate values of SA_{Rock}.

Issues with current SPID method for quantifying epistemic uncertainty

As mentioned previously, following the method outlined in the SPID for quantifying epistemic uncertainty can lead to

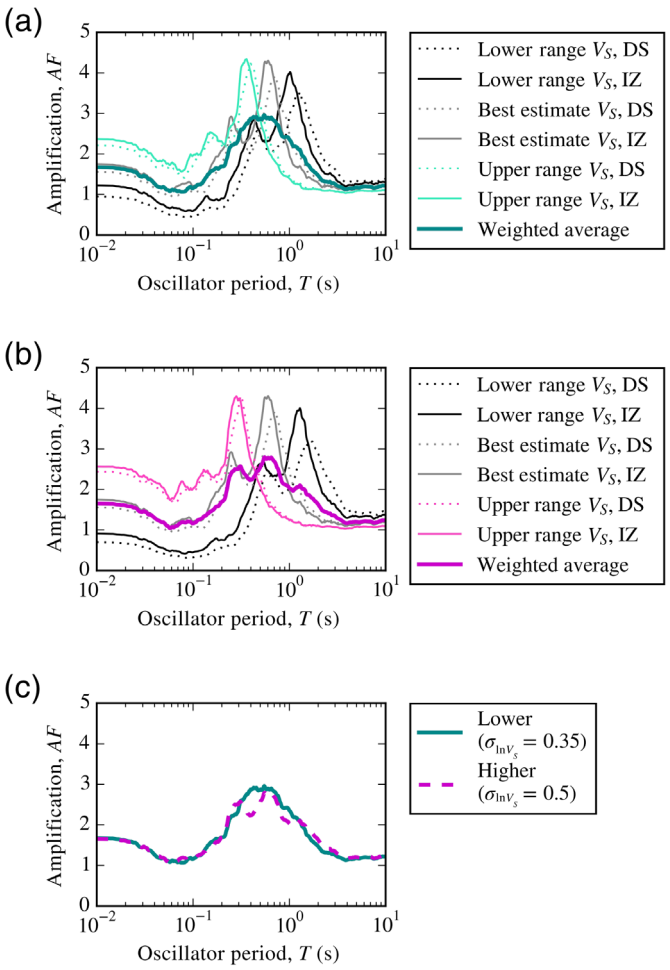

Figure 7. Example mean site amplification, μ_{Total} versus T for two levels of epistemic uncertainty: (a) $\sigma_{\ln V_S} = 0.35$ and (b) $\sigma_{\ln V_S} = 0.5$ for the hypothetical scenario. Shown together in (c). IZ: Ishibashi and Zhang (1993) MRD curve and DS: Darendeli and Stokoe (Darendeli, 2001) MRD curve. The color version of this figure is available only in the electronic edition.

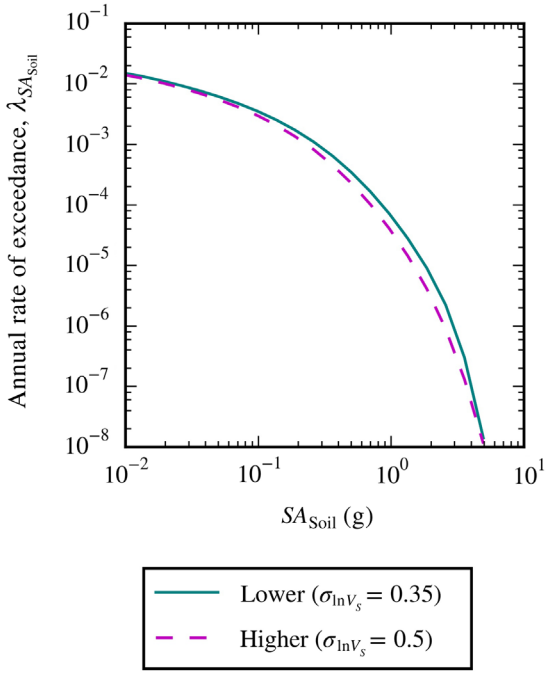

Figure 8. Example $\lambda_{SA_{\text{Soil}}}$ versus SA_{Soil} for two levels of epistemic uncertainty: $\sigma_{\ln V_S} = 0.35$ and $\sigma_{\ln V_S} = 0.5$ using the SPID method for the hypothetical scenario ($T_j = 0.4$ s). The color version of this figure is available only in the electronic edition.

higher mean ground motions when there is lower epistemic uncertainty, which is against the guiding principle that higher uncertainty should generally lead to higher hazard. This issue ultimately stems from the weighted averaging process, which causes a statistical smoothing of the *AF* curve and could lead to a lower peak for the weighted average *AF* despite higher uncertainty. This smoothing represents the uncertainty in the period corresponding to the peak amplification. If the logic-tree weights are taken to be subjective probabilities (Bommer and Scherbaum, 2008), then it is appropriate that the uncertainty of the period at which resonance occurs results in a smoothing of the amplification. In other words, the site-response analyses predict a certain value of peak amplification, but the exact period at which this occurs is not known a priori due to epistemic uncertainty. Consequently, larger epistemic uncertainty implies that the peak amplification could occur over a broader period band, and thus the smoothing is stronger. An example of this issue is shown in Figure 7 for the hypothetical scenario, which shows the weighted average *AF* curves for two levels of epistemic uncertainty: $\sigma_{\ln V_S} = 0.35$ and $\sigma_{\ln V_S} = 0.5$. For some values of T, the value of *AF* is greater for the lower epistemic uncertainty scenario than for the higher epistemic uncertainty scenario. Figure 8 compares the resulting soil hazard curves for $T_j = 0.4$ s and shows that the mean hazard is also larger for the lower epistemic uncertainty scenario.

Although the earlier discussion provides an explanation for the observed reduction in hazard due to larger epistemic uncertainty, such a reduction presents several problems. One problem is that, from an engineering point of view, seismic hazard is only an intermediate step toward the evaluation of risk or losses due to future earthquakes. If risk were linearly proportional to hazard, then an averaging of hazard would imply an equivalent averaging of the risk (e.g., structural response). Whether this averaging is correct or not depends on whether the averaging of the peak response is accepted as an appropriate representation of the hazard. However, this is not the case for strongly nonlinear phenomena, such as structural collapse. Therefore, when the average hazard is propagated to estimate risk, it could result in an underestimation of risk. This problem can be minimized in the analysis of critical facilities (e.g., nuclear power plants) if the risk analysis properly accounts for hazard fractiles, including those that result

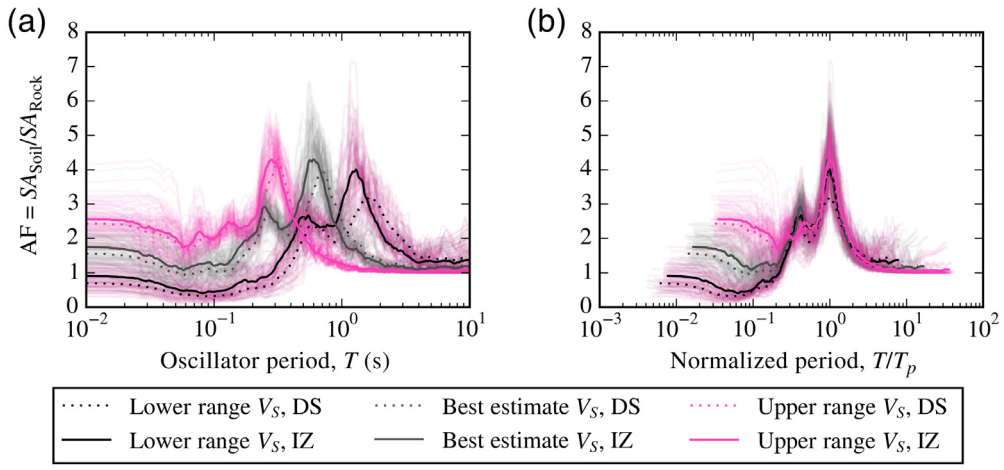

Figure 9. $AF(T)$ curves from individual site-response analyses using a suite of ground motions and all six branches of the SPID logic tree plotted against (a) T and (b) T/T_p. IZ: Ishibashi and Zhang (1993) and DS: Darendeli and Stokoe (Darendeli, 2001). The color version of this figure is available only in the electronic edition.

from the application of a site-response logic tree (Fig. 3). However, for noncritical applications in which only mean hazard is used, this problem will persist.

A second problem associated with the smoothing of amplification peaks due to epistemic uncertainty is related to potential building code applications in which risk computations are performed in a very simplistic manner. The current version of the reference standard for building codes (i.e., ASCE 7-16, American Society of Civil Engineers, 2017) allows for site-specific PSHA. However, there is no specification regarding how logic trees should be implemented within this framework. The hypothetical example discussed previously illustrates a potential problem because it is possible that additional site characterization, meant to reduce epistemic uncertainty, can lead to a higher mean hazard, as shown in Figure 8. This creates a disincentive for performing additional site characterization. For this reason, we adopt the guiding principle stated previously, that, at least for code-based applications, higher epistemic uncertainty should lead to a higher mean hazard.

One additional potential problem with the SPID approach is that it ties the determination of logic-tree weights to the underlying V_S profiles that are then applied to the associated AF curves. We see in Figures 5 and 7 that the resulting shapes of the weighted average AF (Fig. 7) and the weighted standard deviation of AF (Fig. 5) can have local minima that are the result of the use of a limited number of discretized profiles. The desired outcome is to capture the proper distribution of AFs as a result of epistemic uncertainty, not the distribution of V_S profiles. Hence, we recommend that the mean and standard deviation of AF used in hazard computations be determined by evaluating the resulting AFs (in a plot versus period) and not be tied blindly to the underlying V_S profiles (see also Rodriguez-Marek *et al.*, 2020).

PROPOSED ADJUSTMENTS TO THE SPID METHOD

Two alternative methods were investigated as part of this study to resolve the issues with the SPID method: first, a normalization method and, second, an enveloping method. The first solution was found only to be successful for a finite range of scenarios, whereas the second solution was found to be more robust and resolved the issues with the SPID method as desired. These two alternatives are discussed in the following sections.

First solution: Normalization of T using predominant period, T_p

The first proposed solution to the highlighted issues with the current SPID method was to use an approach proposed by Green *et al.* (2016) that is analogous to the binormalization concept proposed by Ziotopoulou and Gazetas (2010) for computing the statistical average of response spectra. In this first proposed approach, the AF curves are conditioned on variables that have a significant influence on the site response, and then these conditioned AF curves are used to compute hazard curves for SA_{Soil}. The variable selected to normalize the AF curves was the predominant period (T_p), which is the oscillator period associated with the maximum value of $AF(T)$. This is illustrated in Figure 9 for the hypothetical scenario. The desired outcome is that the peaks of the AF curves from both lower and higher epistemic uncertainty cases align at the same value of T/T_p. The value of λ_z would then be computed as

$$\lambda_z(a) = \int_0^\infty \int_0^\infty P\left[Y \geq \frac{a}{x} | x, T_p\right] f_{x,T_p}(x, T_p) dx dT_p, \qquad (7)$$

in which $f_{x,Tp}(x, T_p)$ is the joint probability density function of SA_{Rock} and T_p.

This solution was not entirely successful. As shown in Figure 10, this normalization approach resolves the issues with the SPID for some values of λ_z (i.e., SA_{Soil} for the higher epistemic uncertainty scenario is equal to or greater than values of SA_{Soil} for the lower epistemic uncertainty scenario for a given λ_z), but not for all. The change in the hazard curves is not large enough to bring the hazard curve for the higher epistemic uncertainty scenario above the hazard curve for the lower epistemic uncertainty scenario. The reason that this method does not change the hazard results is that the uncertainty in site period in the SPID approach (represented by the three profiles)

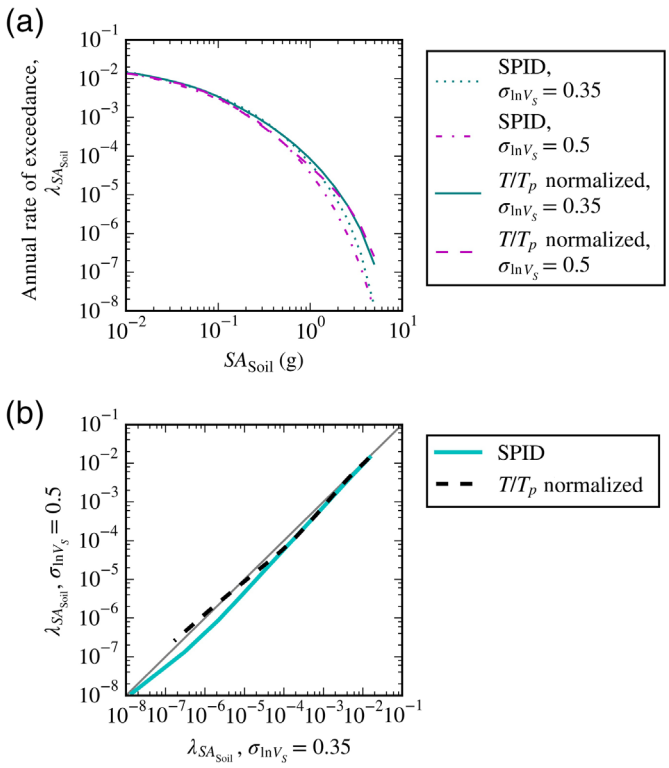

Figure 10. Comparison of $\lambda_{SA_{Soil}}$ for two levels of epistemic uncertainty: $\sigma_{\ln V_S} = 0.35$ and $\sigma_{\ln V_S} = 0.5$ for the hypothetical scenario using the SPID method and the proposed normalization method. Plot (a) shows all four hazard curves, and plot (b) shows direct comparisons of $\lambda_{SA_{Soil}}$ within each described method. $T_j = 0.4$ s. The color version of this figure is available only in the electronic edition.

is replaced by the continuous distribution of the uncertainty on the site period; thus the resulting hazard does not change. Therefore, larger uncertainty in the predominant period of the profile still results in a stronger smoothing of the peak amplification.

Second solution: Envelope approach

Another way to overcome the highlighted issues with the current SPID method is to operate directly on the resulting $AF(T)$ versus T plot and consider an alternative in which the amplitude of the peak is not smoothed by a weighted average. To incorporate this alternative, a separate branch of the logic tree is added, as shown in Figure 11. The purpose of this additional branch is to better preserve the peak of the $AF(T)$ curves when the target T_j is close to T_p. The weighted averaging process in the SPID tends to smooth out this peak, but this additional branch of the logic tree considers an $AF(T)$ that is an envelope of the individual $AF(T)$ values of all of the branches from the SPID logic tree. The period-dependent weight (α) assigned to this additional branch ("envelope branch") will be greater when T_j is closer to T_p and will be close to zero when T_j is far from T_p. The weight assigned to the original logic tree from the SPID method ("SPID branch") is $1 - \alpha$. The actual shape of α as a function of T will be determined by the practitioner performing the analysis, but some recommendations are discussed subsequently.

Development of a relationship for $\alpha(T)$

The main property of the $\alpha(T)$ relationship is that α reaches its maximum when T is equal to the most likely value of T_p (as determined from the site-response analyses from all scenarios in the logic tree) and that α reaches values close to zero when T is far from the most likely value of T_p. The recommended shape is similar to the probability density function of a Gaussian distribution (i.e., bell curve). To apply this shape, assume that T_p is lognormally distributed, and compute its lognormal mean ($\mu_{\ln T_p}$) and standard deviation ($\sigma_{\ln T_p}$) from the amplification factors corresponding to each logic-tree branch. Plot the resulting probability density function (f_{T_p}), and scale or shift the values such that the maximum and minimum values correspond to the desired maximum and minimum values of α. For example, Figure 12 shows the f_{T_p} curve for the hypothetical scenario and the $\alpha(T)$ curve with a maximum value of 1.0 and an asymptotic minimum of 0. The weight α represents a belief that the peak amplification will occur around the best-estimated site period. In some cases, the values of T_p may be affected by the value of SA_{Rock}; in this case, the f_{T_p} curve could be developed as a function of SA_{Rock}. In this scenario, the relationship between T_p and SA_{Rock} was not strong enough to warrant an adjustment to the f_{T_p} curve.

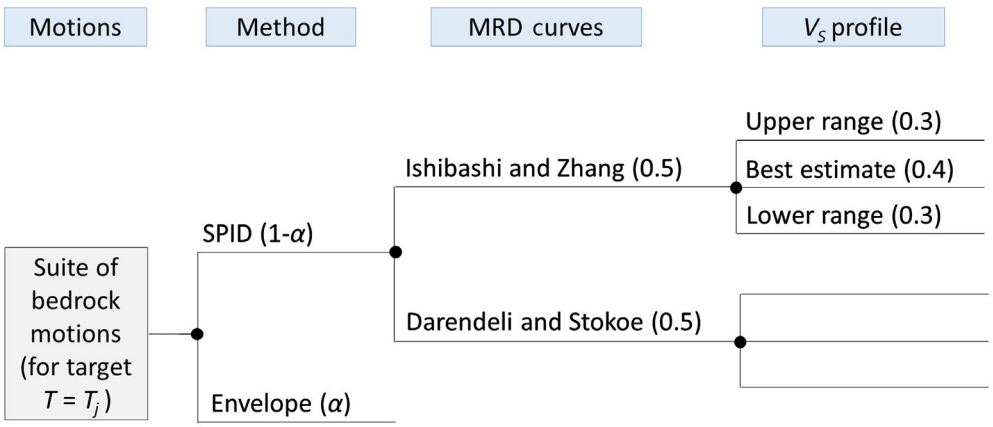

Figure 11. Proposed modified logic tree with the addition of a branch representing the enveloped maximum values of $AF(T)$, in which the weight α is a function of the target period, T_j. The color version of this figure is available only in the electronic edition.

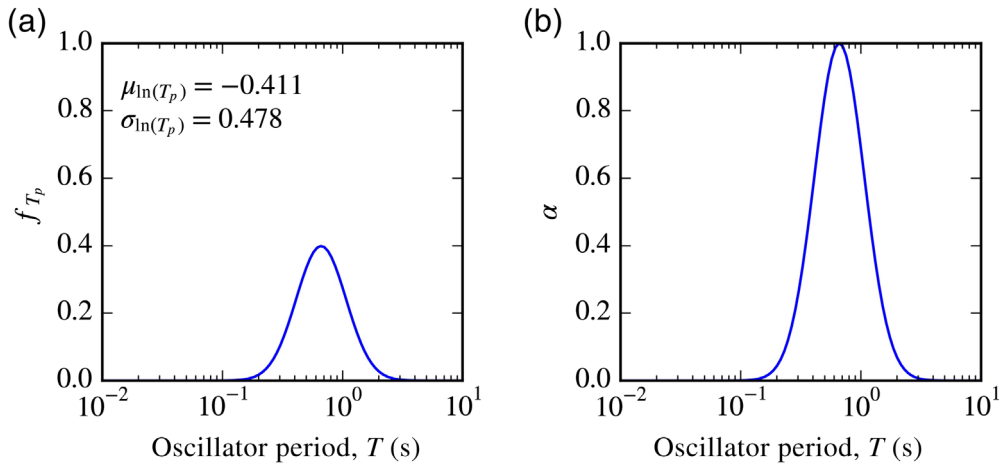

Figure 12. Example of (a) f_{T_p} and (b) $\alpha(T)$ for the proposed method for the hypothetical scenario. The color version of this figure is available only in the electronic edition.

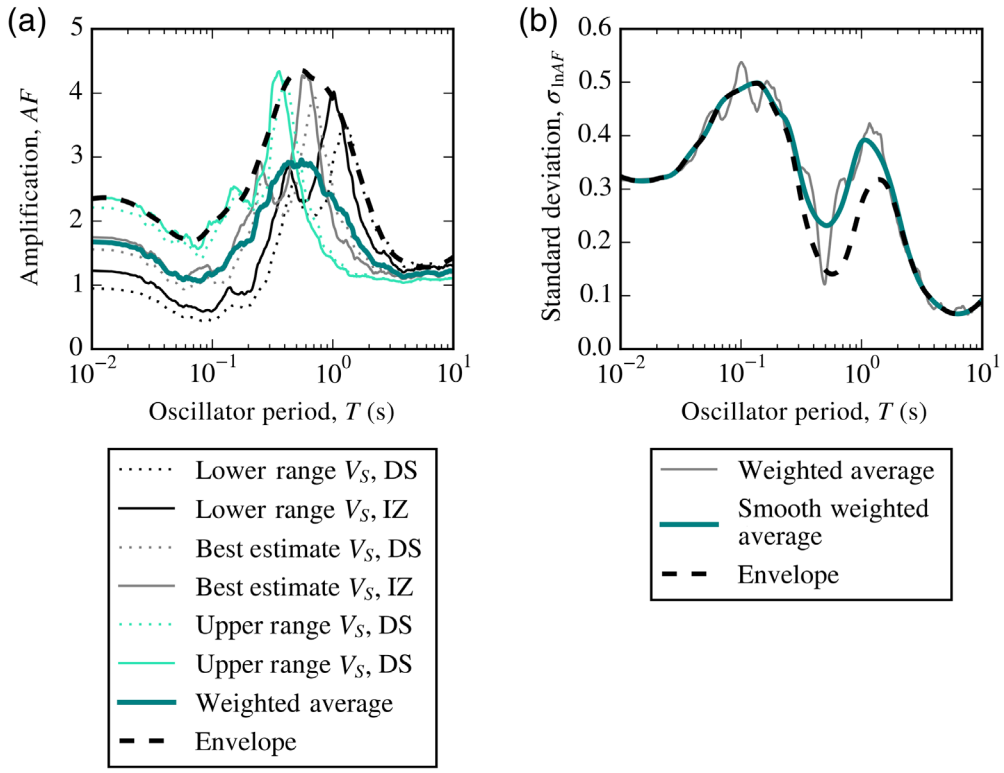

Figure 13. Examples of (a) enveloped $AF(T)$ and (b) enveloped $\sigma_{\ln AF(T)}$ curves for the hypothetical scenario. IZ: Ishibashi and Zhang (1993) MRD curve and DS: Darendeli and Stokoe (Darendeli, 2001) MRD curve. The color version of this figure is available only in the electronic edition.

Development of an envelope for the $AF(T)$ and $\sigma_{\ln AF(T)}$ curves

The first step in developing an envelope for the $AF(T)$ curve is to plot all $AF(T)$ curves from the original logic tree (SPID-recommended) and plot the maximum value from all curves for each value of T. This will likely result in a relatively jagged relationship that may have a few peaks. If the peaks are fairly close, it may be reasonable to make a single peak in the envelope by connecting the peaks with a parabola and then smoothing out the relationship elsewhere using a filter (e.g., Savitzky–Golay filter: Savitzky and Golay, 1964). The natural log of the resulting smoothed envelope is assumed to be the mean $\ln[AF(T)]$ for the envelope branch of the logic tree ($\mu_{\ln Y,\mathrm{Env}}$). An example of an enveloped $AF(T)$ curve is shown in Figure 13a. The value of $\sigma_{\ln AF(T)}$ for the envelope method ($\sigma_{\ln Y,\mathrm{Env}}$) is modified from the smoothed σ_{Total} curve used for the SPID method. The value of $\sigma_{\ln Y,\mathrm{Env}}$ is equal to σ_{Total} when α is equal to 0, and the value of $\sigma_{\ln Y,\mathrm{Env}}$ is equal to a minimum of 0.15 when α reaches its maximum, $\alpha_{\max}$. Written mathematically,

$$\sigma_{\ln Y,\mathrm{Env}}(T) = \sigma_{\mathrm{Total}} - \sigma_{\mathrm{Total}} \left(1 - \frac{0.15}{\sigma_{\mathrm{Total}}(T_{\alpha_{\max}})}\right) \times \frac{\alpha}{\alpha_{\max}}, \quad (8)$$

in which $\sigma_{\mathrm{Total}}(T_{\alpha,\max})$ is the value of σ_{Total} evaluated at the period corresponding to $\alpha_{\max}$ (i.e., $T = \exp[\mu_{\ln T_p}]$). The value of 0.15 represents a judgment on what should be the minimum epistemic uncertainty assigned to the uncertainty in site amplification (Rodriguez-Marek *et al.*, 2014; Bommer *et al.*, 2015). An example of an enveloped $\sigma_{\ln Y,\mathrm{Env}}$ is compared with σ_{Total} in Figure 13b.

Modified site-specific soil hazard curves for SA_{Soil}

To compute site-specific soil hazard curves for SA_{Soil} using this modified method, the hazard integral is computed for both

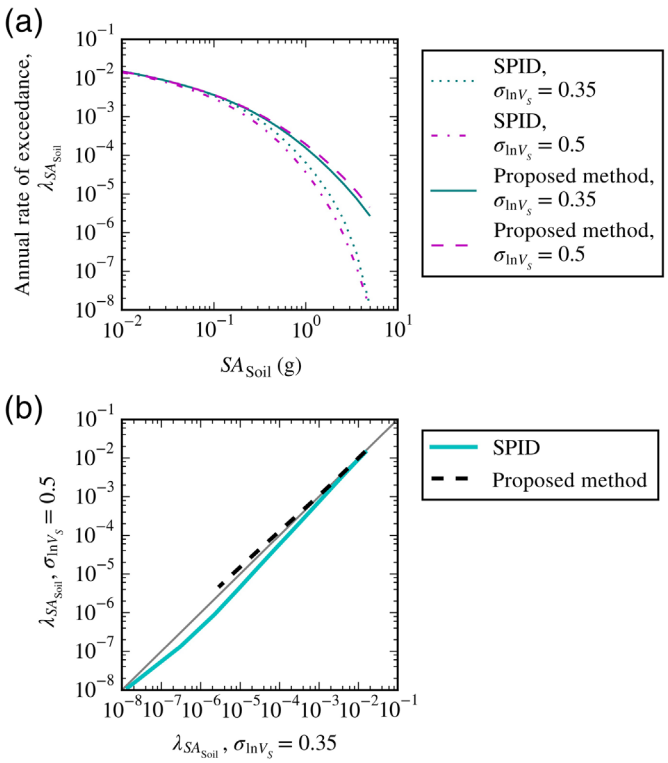

Figure 14. Comparison of $\lambda_{SA_{Soil}}$ for two levels of epistemic uncertainty: $\sigma_{\ln V_S} = 0.35$ and $\sigma_{\ln V_S} = 0.5$ for the hypothetical scenario using the SPID method and the proposed modified method. Plot (a) shows all four hazard curves, and plot (b) shows direct comparisons of $\lambda_{SA_{Soil}}$ within each described method. The color version of this figure is available only in the electronic edition.

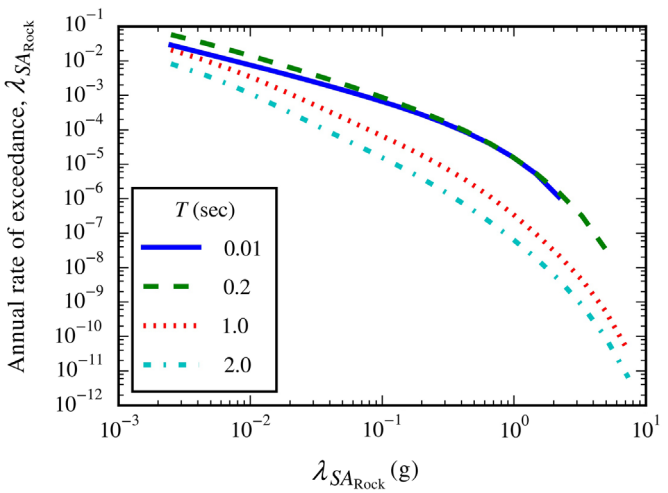

Figure 15. Seismic hazard curves for rock motions at the case history site (U.S. Geological Survey Unified Hazard Tool, site class A). The color version of this figure is available only in the electronic edition.

branches: the SPID branch and the envelope branch. The integral required to estimate $\lambda_z(a)$ for the SPID branch was given as equation (4) and is hereafter denoted $\lambda_{z,\mathrm{Avg}}(a)$. The discretized form of the integral required to estimate the annual rate of exceedance for SA_{Soil} for the envelope branch ($\lambda_{z,\mathrm{Env}}(a)$) is

$$\lambda_{z,\mathrm{Env}}(a) = \sum_{x_k} P\left[Y \geq \frac{a}{x_k}|x_k\right]_{\mathrm{Env}} p_x(x_k), \tag{9}$$

$$P[Y \geq \frac{a}{x_k}|x_k]_{\mathrm{Env}} = 1 - \Phi\left(\frac{\ln(\frac{a}{x_k}) - \mu_{\ln Y,\mathrm{Env}}}{\sigma_{\ln Y,\mathrm{Env}}}\right), \tag{10}$$

in which $\mu_{\ln Y,\mathrm{Env}}$ and $\sigma_{\ln Y,\mathrm{Env}}$ are from the envelopes developed previously. Here, we assume that $\mu_{\ln Y,\mathrm{Env}}$ and $\sigma_{\ln Y,\mathrm{Env}}$ are independent of $SA_{\mathrm{Rock}}(T_j)$. Finally, the following equation is used to compute the composite value of $\lambda_z(a)$ using both the SPID and envelope branches:

$$\lambda_z(a) = \alpha \times [\lambda_{z,\mathrm{Env}}(a)] + (1-\alpha) \times [\lambda_{z,\mathrm{Avg}}(a)], \tag{11}$$

in which α depends on the target T_j and the practitioner's judgment. If the maximum value of α is 1.0, then for target T_j values close to the most likely value of T_p, $\lambda_z(a) \approx \lambda_{z,\mathrm{Env}}(a)$.

Figure 14 compares $\lambda_{z,\mathrm{Avg}}$ from the SPID method and $\lambda_{z,\mathrm{Env}}$ from the proposed modified method for lower and higher epistemic uncertainties using the hypothetical scenario, and it is shown that the modified method fixes the problem associated with the SPID method. Specifically, the mean hazard for the lower epistemic uncertainty case does not exceed the mean hazard for the higher epistemic uncertainty case. The following section compares results of the SPID method and this proposed method using a case history.

COMPARISONS BETWEEN SPID METHOD AND MODIFIED METHOD: CASE HISTORY

A site in the eastern United States was selected to highlight the previously discussed issue with the current SPID method and to compare with results using the proposed method in this study. The exact location of the site is not given herein due to confidentiality. However, some of the assumptions provided in the original project report are used herein for simplicity.

PSHA for rock motions and input ground-motion selection

The PSHA for rock motions ($\lambda_x = \lambda_{SA_{\mathrm{Rock}}}$) was retrieved from the "Unified Hazard Tool" website provided by the USGS using approximate geographic coordinates for the site and selecting site class A to represent V_S of the bedrock (Fig. 15). The resulting uniform hazard spectra (UHS) values for the four return periods (T_r) of 475, 1000, 1500, and 2500 yr are shown in Figure 16. A suite of 11 ground motions was selected from the Next Generation Attenuation (NGA) databases: NGA-West2

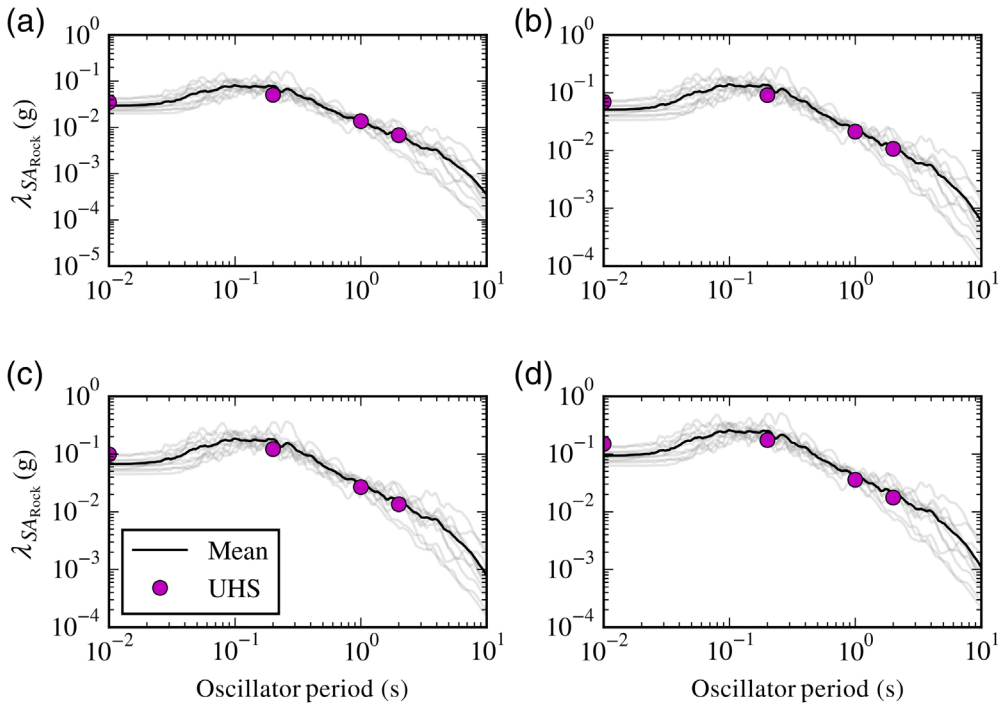

Figure 16. Uniform hazard spectra values compared with response spectra from the suite of 11 scaled rock motions (5% damping) using four return periods: (a) 475, (b) 1000, (c) 1500, and (d) 2500 yr. The color version of this figure is available only in the electronic edition.

and NGA-East (Pacific Earthquake Engineering Research Center [PEER], "PEER Ground Motion Database," see Data and Resources) and linearly scaled to match the UHS values. In doing so, we assume that the primary factor controlling the AF is the input motion intensity (i.e., SA_{Rock}; Bazzurro and Cornell, 2004a). Alternative ground-motion and scaling approaches that match specific scenarios (i.e., in terms of magnitude and distance) at different return periods could have been used (e.g., Bradley, 2012); however, we opted for a simpler approach because ground-motion selection is not a focus of this study. A summary of these 11 ground motions and the scaling factors for each return period are given in Table 1, and their response spectra are compared with the UHS values in Figure 16.

V_S profiles, MRD curves

A series of borings and nine seismic cone penetration tests (SCPTs) were performed at the case history site. V_S was estimated using SCPTs where possible (none extended deeper than 20 m); otherwise, correlations with the results from the borings were used to estimate V_S. Bedrock was assumed to be located at 42.7 m depth with $V_S = 2438$ m/s. The SCPTs were also used to estimate $\sigma_{\ln V_S}$ with depth, and it was found that for depths shallower than 18.3 m the value of $\sigma_{\ln V_S}$ was less than the default SPID value of 0.35 for sites with limited soil testing. This justified using lower values of $\sigma_{\ln V_S}$ for some soil layers, but not all. Table 2 summarizes

TABLE 1
Scaling Factors Used for the Suite of 11 Rock Motions

Earthquake and Year	NGA Number	Magnitude M_w	Station Name, Component	Scaling Factor $T_r = 475$ yr	$T_r = 1000$ yr	$T_r = 1500$ yr	$T_r = 2500$ yr
California/Baja border area, 2002	2003	5.31	Calexico Fire Station, 90	0.30	0.52	0.69	0.97
Chi-Chi, Taiwan, 1999	2949	6.20	CHY033, E	0.37	0.63	0.83	1.16
			CHY033, N	0.36	0.62	0.82	1.14
	2985	6.20	CHY094, W	0.39	0.67	0.88	1.23
			CHY094, N	0.39	0.67	0.88	1.24
Mineral, Virginia, 2011	8529	5.74	NP2555, E	0.47	0.80	1.06	1.48
			NP2555, N	1.03	1.77	2.33	3.27
Morgan Hill, 1984	455	6.19	Gilroy Array Number 1, 230	0.49	0.85	1.12	1.56
			Gilroy Array Number 1, 320	0.34	0.59	0.77	1.08
Whittier Narrows, 1987	624	5.99	Huntington Beach, 270	0.61	1.05	1.39	1.95
			Huntington Beach, 360	0.49	0.83	1.1	1.54

E, east; N, north; NGA, Next Generation Attenuation; W, west.

the soil layering, the best estimate V_S, and the maximum value of $\sigma_{\ln V_S}$ for each soil layer at the case history site.

Figure 17 shows the best estimate V_S profile with depth and the corresponding upper and lower ranges using $\sigma_{\ln V_S}$ for two scenarios: $\sigma_{\ln V_S} \leq 0.35$ (as given in Table 2) and $\sigma_{\ln V_S} = 0.50$. This site would be considered to have an intermediate level of epistemic uncertainty in terms of the V_S profile (due to the absence of direct measurements at depths greater than 20 m, but with a good degree of geotechnical site characterization), but for comparison purposes this study will consider the more extreme scenario. The V_S of the bedrock was not changed for the upper and lower range V_S profiles. The purpose of maintaining the same V_S of the bedrock was to focus only on the effects of epistemic uncertainty on the site response of the soil above the bedrock. A more elaborate analysis would be needed to consider the depth and the V_S of the bedrock by including additional nodes in the logic tree.

The two sets of MRD curves that were selected for this study were Darendeli and Stokoe (Darendeli, 2001) and Ishibashi and Zhang (1993). Each set was applied to all soil layers, depending on the branch of the logic tree being used. These MRD curves are functions of mean effective stress and plasticity index (PI) or soil type. In turn, mean effective stress is a function of unit weight of the soil, depth to groundwater, and lateral earth pressure coefficient, which were assumed to be 19 kN/m^3, 1.8 m, and 0.5, respectively, for all soil layers. The PI was equal to 65 and 15 for the former river deposits and the clay to clayey silt layers, respectively, and PI was equal to zero for all other soil layers.

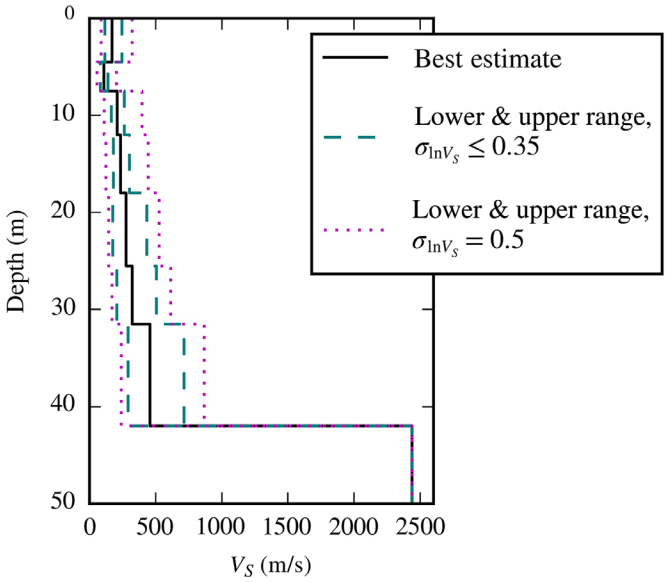

Figure 17. Best estimate, lower- and upper-range V_S profiles (i.e., median, 10th and 90th percentiles) for the case history site where $\sigma_{\ln V_S} = 0.35$ or $\sigma_{\ln V_S} = 0.5$. The color version of this figure is available only in the electronic edition.

Comparisons of smoothed $AF(T)$ and $\sigma_{\ln AF(T)}$ curves

Figure 18 shows the weighted average $AF(T)$ curve for the SPID method compared with the enveloped $AF(T)$ curve used in the additional branch of the proposed method in this study for the two epistemic uncertainty scenarios. This plot does not sample AF as a function of SA_{Rock}. Figure 19 shows the smoothed weighted average standard deviation of $\ln[AF(T)]$ for the SPID method (σ_{Total}), assuming no motion-to-motion uncertainty in the $AF(T)$ values, compared with the enveloped values used in the additional branch of the proposed method in this study ($\sigma_{\ln,\text{Env}}$). The $\sigma_{\ln AF}$ values are generally higher for the higher epistemic uncertainty scenario, as expected. The probability density function of T_p and the resulting $\alpha(T)$ are shown in Figures 20 and 21, respectively (assigning a maximum value of $\alpha(T)$ as 1.0 and a minimum as 0). The width of the $\alpha(T)$ curve for the higher epistemic uncertainty scenario is larger than the width for the lower epistemic uncertainty scenario, as expected.

Comparisons of probabilistic site-specific hazard curves: SPID and proposed method

Figure 22 compares the probabilistic site-specific soil hazard curves for SA_{Soil} (for $T_j = 0.4$ s) using the SPID method

TABLE 2
Assumed Layering, Best Estimate V_S Profile, and Site-Specific Estimates of $\sigma_{\ln V_S}$ for Each Soil Layer at the Case History Site

Layer	Source	Layer Thickness (m)	Best Estimate V_S (m/s)	$\sigma_{\ln V_S}$
Fill	Borings, SCPT	4.6	170	0.29
Former river deposits		3.0	108	0.20
Silt to silty sand 1		4.6	210	0.18
Silt to silty sand 2		6.1	234	0.20
Clay to clayey silt 1		7.6	277	0.35*
Clay to clayey silt 2		6.1	323	0.35*
Sand and gravel	Borings	10.7	457	0.35*
Bedrock	Assumed	N/A	2438*	N/A

SCPT, seismic cone penetration test.
*Assumed value.

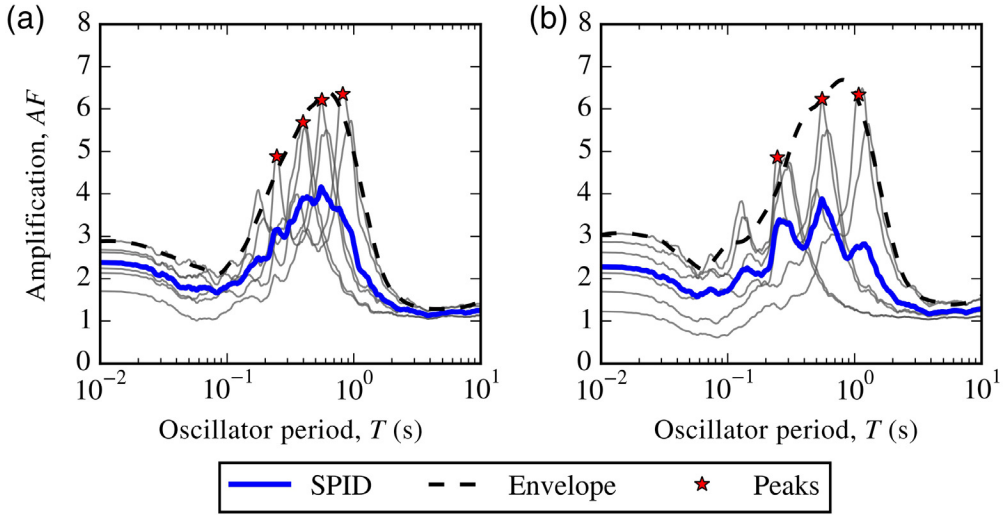

Figure 18. $AF(T)$ curves for the SPID method and the additional branch of the new proposed method ("Envelope") for the case history site for two levels of epistemic uncertainty: (a) $\sigma_{\ln V_s} \leq 0.35$ and (b) $\sigma_{\ln V_s} = 0.50$. Gray lines represent mean $AF(T)$ curves for individual branches of the SPID-recommended logic tree, and red stars represent peaks used to smooth the "Envelope" curve. The color version of this figure is available only in the electronic edition.

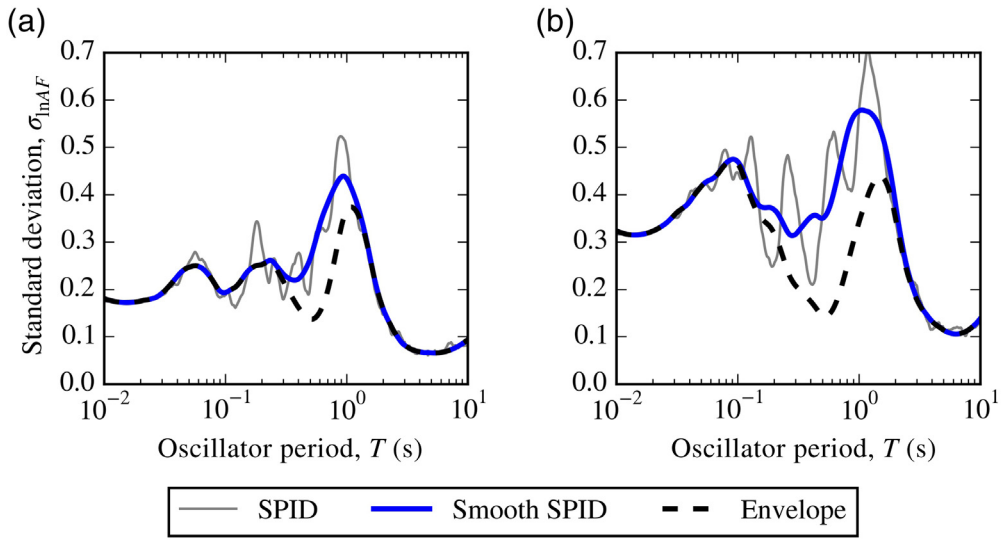

Figure 19. $\sigma_{\ln AF(T)}$ curves for the SPID method ("Smooth SPID") and the additional branch of the new proposed method ("Envelope") for two levels of epistemic uncertainty: (a) $\sigma_{\ln V_s} \leq 0.35$ and (b) $\sigma_{\ln V_s} = 0.50$. The color version of this figure is available only in the electronic edition.

and the proposed method in this study. The mean hazard from the SPID method for the lower epistemic uncertainty case is higher than the mean hazard for the higher epistemic uncertainty case for nearly all values of SA_{Soil}. However, using the proposed method, the mean hazard for the lower epistemic uncertainty case no longer exceeds the mean hazard for the higher epistemic uncertainty case. Thus, for this oscillator period, the proposed method addresses the shortcoming of the SPID method as intended. An additional outcome of the proposed method is that the computed mean hazard is generally higher than the mean hazard computed using the SPID method. This is because $T_j = 0.4$ s is near the most likely value of T_p (≈0.5 s), which led to a higher value of α and a more significant weight given to the enveloped $AF(T)$ curve compared with the weighted average $AF(T)$ curve. This generally increases the value of $AF(T_j)$ for $T_j = 0.4$ s in the hazard integral, which shifts the hazard curve of SA_{Soil} upward. This result reflects the analyst's belief that the predicted peak amplification is likely to be realized for the best-estimated site period. As discussed earlier in this article, the higher hazards existing near the best-estimated site period is a desired outcome for cases in which hazard fractiles are not used in risk analysis. For other target T_j values far from the most likely value of T_p, the upward shift will be almost nonexistent (i.e., the hazard curves from the SPID method and the proposed method will be nearly identical).

Table 3 compares the SA_{Soil} values associated with four values of T_j: 0.4, 0.6, 1.0, and 2.0 s, for two return periods, T_r: 100 and 2000 yr. As mentioned previously, when $T_j = 0.4$ s, the SPID method produces higher values of SA_{Soil} when epistemic uncertainty is low, but the proposed method reverses this issue. For $T_j = 0.6$ s, the SPID method again produces higher values of SA_{Soil} when epistemic uncertainty is low, but the proposed method does not entirely reverse this issue. It does, however, make the SA_{Soil} values from the lower and higher epistemic uncertainty scenarios nearly equal. When $T_j = 1.0$ s, the SPID method

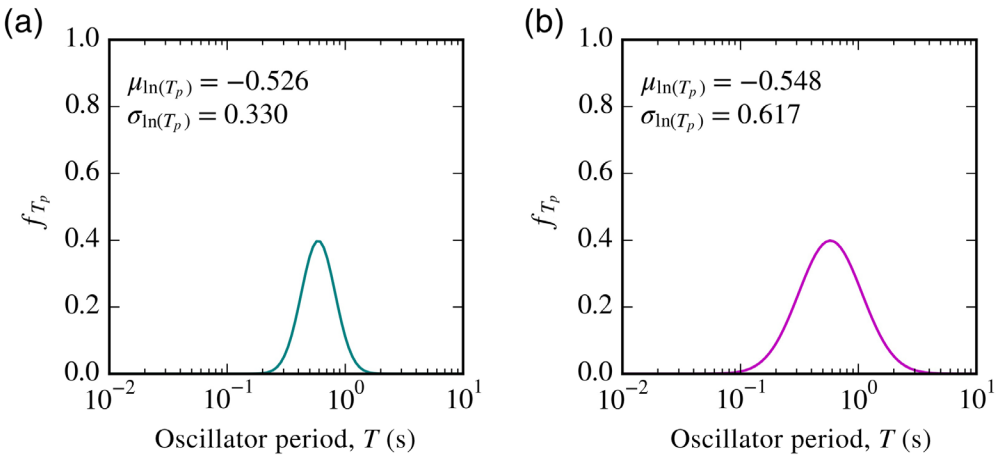

Figure 20. Example f_{T_p} curves for the new proposed method for two levels of epistemic uncertainty: (a) $\sigma_{\ln V_S} \leq 0.35$ and (b) $\sigma_{\ln V_S} = 0.50$. The color version of this figure is available only in the electronic edition.

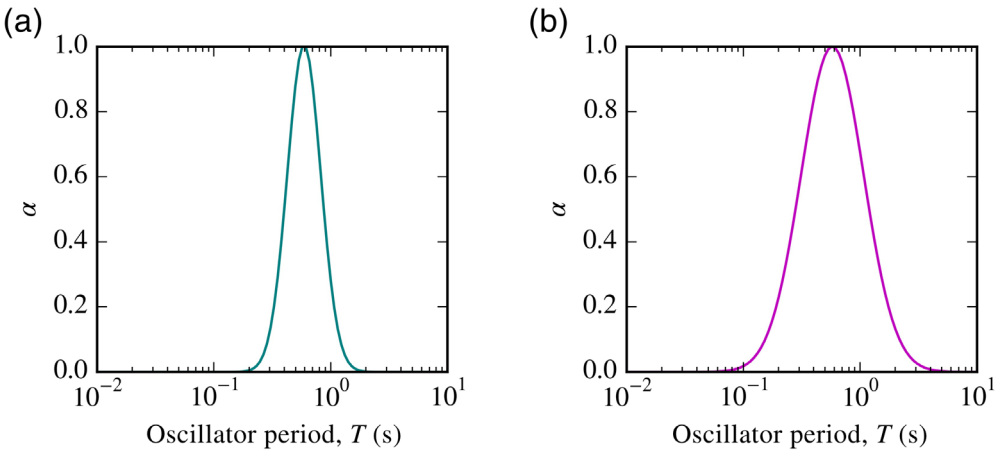

Figure 21. Example $\alpha(T)$ curves for the new proposed method for two levels of epistemic uncertainty: (a) $\sigma_{\ln V_S} \leq 0.35$ and (b) $\sigma_{\ln V_S} = 0.50$. The color version of this figure is available only in the electronic edition.

appropriately assigns lower values of SA_{Soil} to the lower epistemic uncertainty scenario, and so does the proposed method (though with higher values of SA_{Soil}). When $T_j = 2.0$ s, the SPID method and the proposed method yield similar values of SA_{Soil} because the value of T_j is sufficiently far from the most likely value of T_p that the weight given to the enveloped $AF(T)$ curve is nearly equal to zero.

CONCLUSIONS

This study shows that using a weighted average approach using scaled V_S profiles, as outlined in the SPID, to account for epistemic uncertainty in soil properties as part of a site-response analysis in a PSHA can lead to statistical smoothing of the $AF(T)$ curve and to decreased hazard as epistemic uncertainty increases. We postulate that, for cases when the mean hazard is used for design (i.e., in typical practice scenarios), a guiding principle should be that higher uncertainty should lead to higher hazard. Because the SPID approach can result in hazard that violates this principle, it reduces the incentive for practitioners to thoroughly characterize soil properties at a site. The alternative method proposed in this study retains the simplicity implicit in code-based approaches while preserving the peak behavior of the $AF(T)$ curve. This method allows the practitioner to use judgment to assign weights to the enveloped $AF(T)$ curve based on how well the peaks of the $AF(T)$ curve are captured. Because the weights are intended to be period dependent, the differences in the hazard curves from the SPID method and the proposed method will also be period dependent. The proposed method was shown to improve the issue with the SPID method for at least two targeted periods and to yield results similar to the SPID method for two other periods in which the highlighted issue was nonexistent. In this study, we also identify potential issues with carrying logic-tree weights on V_S profiles directly into hazard results. We recommend that the mean and standard deviation of AF used in hazard computations be determined by evaluating the resulting AFs (in a plot versus period), and not be tied blindly to the underlying V_S profiles.

DATA AND RESOURCES

The probabilistic seismic hazard analysis (PSHA) for rock was obtained from the U.S. Geological Survey (USGS) Unified Hazard Tool, https://earthquake.usgs.gov/hazards/interactive/ (last accessed June 2019). Strong ground motion acceleration time histories were obtained from the Next Generation Attenuation (NGA) databases: NGA-West2 and NGA-East, https://ngawest2.berkeley.edu/ (last accessed June 2019). Geotechnical data for the case history are proprietary and cannot be publicly released. All other data used in this article came from published sources listed in the references.

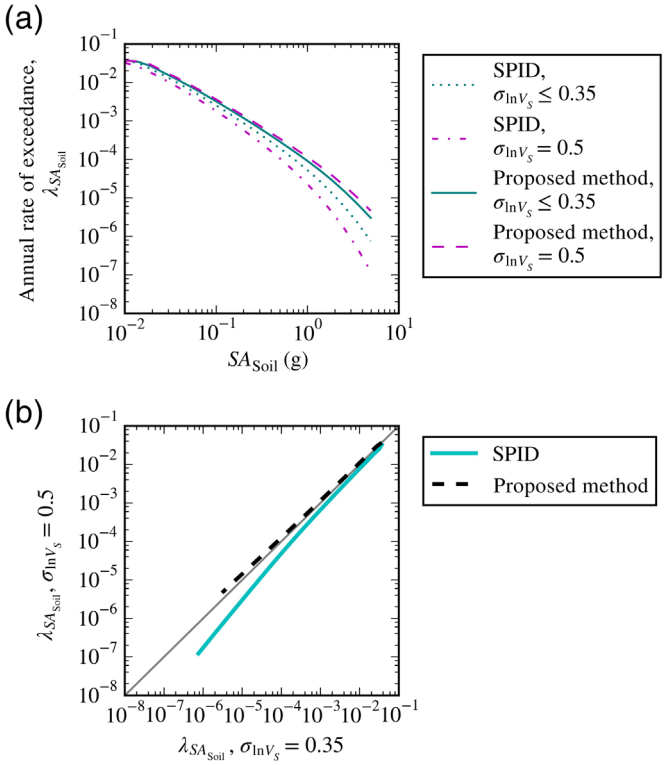

Figure 22. Comparisons of the SPID method and the proposed method for the case history site in (a) hazard curves and (b) direct comparisons of annual rates of exceedance (target period is 0.4 s, maximum α for new method is 1.0). The color version of this figure is available only in the electronic edition.

DECLARATION OF COMPETING INTERESTS

The authors acknowledge that there are no conflicts of interest recorded.

ACKNOWLEDGMENTS

This article is based upon work supported by the U.S. Geological Survey (USGS) under Grant Number G17AP00011 and U.S. National Science Foundation (NSF) Grants CMMI-1825189 and CMMI-1937984. The views and conclusions contained in this document are those of the authors and should not be interpreted as representing the opinions or policies of the USGS or NSF. The mention of trade names or commercial products does not constitute their endorsement by the USGS.

The authors benefited from discussions about this research with Konstantinos Garcia-Syngros, Langan Engineering, and Emily Gibson, formerly with the U.S. Defense Nuclear Facilities Safety Board (DNFSB). The authors gratefully acknowledge these discussions. However, any opinions, findings, and conclusions or recommendations expressed in this article are those of the authors and do not necessarily reflect the views of others.

REFERENCES

American Society of Civil Engineers (2017). *ASCE/SEI 7-16: Minimum Design Loads and Associated Criteria for Buildings and Other Structures*, Reston, Virginia, doi: 10.1061/9780784414248.

Bazzurro, P., and C. A. Cornell (2004a). Ground-motion amplification in nonlinear soil sites with uncertain properties, *Bull. Seismol. Soc. Am.* **94,** no. 6, 2090–2109.

Bazzurro, P., and C. A. Cornell (2004b). Nonlinear soil-site effects in probabilistic seismic hazard analysis, *Bull. Seismol. Soc. Am.* **94,** no. 6, 2110–2123.

Bommer, J. J., and F. Scherbaum (2008). The use and misuse of logic trees in probabilistic seismic hazard analysis, *Earthq. Spectra* **24,** no. 4, 997–1009.

Bommer, J. J., K. J. Coppersmith, R. T. Coppersmith, K. L. Hanson, A. Mangongolo, J. Neveling, E. M. Rathje, A. Rodriguez-Marek, F. Scherbaum, R. Shelembe, P. Stafford, and F. O. Strasser (2015). A SSHAC Level 3 probabilistic seismic hazard analysis for a new-build nuclear site in South Africa, *Earthq. Spectra* **31,** no. 2, 661–698.

Bradley, B. A. (2012). A ground motion selection algorithm based on the generalized conditional intensity measure approach, *Soil Dynam. Earthq. Eng.* **40,** 48–61.

Chiou, B. S.-J., and R. R. Youngs (2014). Update of the Chiou and Youngs NGA model for the average horizontal component of peak ground motion and response spectra, *Earthq. Spectra* **30,** no. 3, 1117–1153.

Cramer, C. H. (2003). Site-specific seismic-hazard analysis that is completely probabilistic, *Bull. Seismol. Soc. Am.* **93,** no. 4, 1841–1846.

TABLE 3
SA_{Soil} for Return Periods of 100 or 2000 yr Using the Screening, Prioritization, and Implementation Details (SPID) Method and Proposed New Method (with Maximum α of 1.0) for Lower and Higher Epistemic Uncertainties

	SA_{Soil} (g), $T_r = 100$ yr				SA_{Soil} (g), $T_r = 2000$ yr			
	SPID		New		SPID		New	
Target Period, T_j (s)	Lower	Higher	Lower	Higher	Lower	Higher	Lower	Higher
0.4	0.037	0.031	0.043	0.046	0.284	0.216	0.353	0.393
0.6	0.031	0.027	0.043	0.042	0.204	0.181	0.318	0.317
1.0	0.013	0.015	0.016	0.027	0.096	0.099	0.124	0.193
2.0	N/A	N/A	N/A	N/A	0.022	0.027	0.022	0.031

Higher, higher epistemic uncertainty; lower, lower epistemic uncertainty; N/A, lowest value of T_r in hazard curve is greater than 100 yr.

Darendeli, M. B. (2001). Development of a new family of normalized modulus reduction and material damping curves, *Ph.D. Dissertation*, The University of Texas at Austin, Austin, TX.

Der Kiureghian, A., and O. Ditlevsen (2009). Aleatory or epistemic? Does it matter?, *Struct. Saf.* **31,** 105–112.

Electrical Power Research Institute (EPRI) (1993). *Guidelines for Determining Design Basis Ground Motions*, EPRI TR-102293, Vols. 1/5, Electrical Power Research Institute, Palo Alto, California.

Electrical Power Research Institute (EPRI) (2012). *Seismic Evaluation Guidance: Screening, Prioritization and Implementation Details (SPID) for the Resolution of Fukushima Near-Term Task Force Recommendation 2.1: Seismic*, Report 1025287, Electrical Power Research Institute, Palo Alto, California, 206 pp.

Goulet, C. A., and J. P. Stewart (2009). Pitfalls of deterministic application of nonlinear site factors in probabilistic assessment of ground motions, *Earthq. Spectra* **25,** no. 3, 541–555.

Green, R. A., E. Gibson, and A. Rodriguez-Marek (2016). Treatment of epistemic uncertainty in site effects in probabilistic seismic hazard analyses, *Proc. of the 2nd Workshop on Earthquakes in North Iceland*, Húsavík Academic Centre, Húsavík, Iceland, 31 May–3 June, 85–88.

Ishibashi, I., and X. Zhang (1993). Unified dynamic shear moduli and damping ratios of sand and clay, *Soils Found.* **33,** no. 1, 182–191.

Keefer, D. L., and S. E. Bodily (1983). Three-point approximations for continuous random variables, *Manag. Sci.* **29,** no. 5, 595–609.

Rodriguez-Marek, A., J. J. Bommer, R. R. Youngs, M. J. Crespo, P. J. Stafford, and M. Bahrampouri (2020). Capturing epistemic uncertainty in site response, *Earthq. Spectra* doi: 10.1177/8755293020970975.

Rodriguez-Marek, A., E. M. Rathje, J. J. Bommer, F. Scherbaum, and P. J. Stafford (2014). Application of single-station sigma and site response characterization in a probabilistic seismic hazard analysis for a new nuclear site, *Bull. Seismol. Soc. Am.* **104,** no. 4, 1601–1619.

Savitzky, A., and M. J. E. Golay (1964). Smoothing and differentiation of data by simplified least squares procedures, *Anal. Chem.* **36,** no. 8, 1627–1639.

Silva, W. J., N. Abrahamson, G. Toro, and C. Costantino (1996). *Description and validation of the stochastic ground motion model*, *Report submitted to Brookhaven National Laboratory, Associated Universities, Inc., Contract Number 770573*, Upton, New York.

Stewart, J. P., and K. Afshari (2020). Uncertainty in site response as derived from one-dimensional ground response analysis, *J. Geotech. Geoenviron. Eng.* **147,** no. 1, 04020146.

Stewart, J. P., K. Afshari, and Y. M. A. Hashash (2014). Guidelines for performing hazard-consistent one-dimensional ground response analysis for ground motion prediction, *PEER Report 2014/16*, Pacific Earthquake Engineering Research Center, University of California Berkeley, Berkeley, California.

Walling, M., W. Silva, and N. Abrahamson (2008). Nonlinear site amplification factors for constraining the NGA models, *Earthq. Spectra* **24,** no. 1, 243–255.

Ziotopoulou, K., and G. Gazetas (2010). Are current design spectra sufficient for soil-structure systems on soft soils?, in *Advances in Performance-Based Earthquake Engineering*, M. N. Fardis (Editor), chap. 8, Springer, 79–87.

Manuscript received 29 October 2020
Published online 11 May 2021